CERN-TH.5062/88
SCIPP-88/29

COSMIC RAY CONSTRAINTS ON THE ANNIHILATIONS OF RELIC PARTICLES IN THE GALACTIC HALO

John Ellis and R.A. Flores*)
CERN - Geneva

K. Freese
Dept. of Physics, MIT
Cambridge, MA 02138, U.S.A.

S. Ritz+)
University of Wisconsin
Madison, WI 53706, U.S.A.

D. Seckel§)
University of California
Santa Cruz, CA 95064, U.S.A.

and

Joseph Silk
University of California
Berkeley, CA 94720, U.S.A.

ABSTRACT

We re-evaluate the fluxes of cosmic ray antiprotons, positrons and gamma rays to be expected from the annihilations of relic particles in the galactic halo. We stress the importance of observational constraints on the possible halo density of relic particles, and specify their annihilation cross-sections by the requirement that their cosmological density close the Universe. We use a Monte Carlo programme adapted to fit e^+e^- data to calculate the $\bar{p}$, e^+ and γ spectra for some supersymmetric relic candidates. We find significantly smaller $\bar{p}$ fluxes than previously estimated, and conclude that present upper limits on cosmic ray $\bar{p}$ and e^+ do not exclude any range of sparticle masses. We discuss the prospects for possible future constraints on sparticles from cosmic γ rays.

---

*)Address after September 1st, 1988: School of Physics and Astronomy, University of Minnesota, Minneapolis, MN 55455.

+)Address after September 1st, 1988: Department of Physics, Columbia University, New York, NY 10027.

§)Address after September 1st, 1988: Bartol Research Foundation, University of Delaware, Newark, DE 19716.

CERN-TH.5062/88
SCIPP-88/29
May 1988

Astrophysical observations [1] strongly suggest that galactic haloes contain dark matter which has not dissipated like the conventional matter in the galactic disc, and is likely to be non-baryonic [2]. There is no shortage of particle physics candidates for this dark matter, with three of the most favoured being massive neutrinos, axions and relic supersymmetric particles [3,4]. Experimental physicists are now devising strategies for detecting these different species of relic particles. They have been offered three possible signatures of heavy dark matter particles χ such as massive neutrinos or supersymmetric particles. These are χ scattering off nuclei in the laboratory which may produce detectable nuclear recoil energy and/or inelastic nuclear excitation [5], annihilations of relic particles χ trapped in the Sun which may produce an observable flux of high energy solar neutrinos [6], and annihilations of relics χ in the halo which may produce detectable fluxes of antiprotons [7], positrons and gamma rays [7,8]. New data have recently become available from non-dedicated detectors which may constrain some relic particle candidates. These include upper limits on dark matter scattering rates in ^{76}Ge detectors [9] - which exclude Dirac neutrinos ν_D or sneutrinos $\tilde{\nu}$ with masses between 12 and 10^3 GeV if they have the expected halo density, upper limits on high-energy solar neutrinos [10] - which exclude $\tilde{\nu}_e$ or $\tilde{\nu}_\mu$ with masses between $\sim 2\frac{1}{2}$ GeV and 25 GeV but do not exclude any range of photino $\tilde{\gamma}$ or higgsino $\tilde{h}$ masses [11], and new upper limits on the low-energy cosmic ray $\bar{p}$ flux [12] whose implications we analyze in this paper.

The observation of a surprisingly high flux of low-energy $\bar{p}$'s in the cosmic rays a few years ago [13] was very difficult to understand in terms of secondary $\bar{p}$ production by matter cosmic ray primaries [14], and its origin was the subject of many speculations. A particularly interesting suggestion [7] was the idea that these $\bar{p}$'s could be due to relic particle annihilations in the galactic halo: $\chi\chi \to \bar{p}+X$. By making favourable choices of uncertain astrophysical parameters such as the relic halo density ρ_χ^h and the confinement time $\tau_{\bar{p}}$ of $\bar{p}$'s in the galactic magnetic field, it appeared possible [8] to reproduce the claimed flux of $\bar{p}$'s with the annihilations of Dirac neutrinos ν_D or higgsinos $\tilde{h}$, but this was more difficult with photinos $\tilde{\gamma}$, and impossible with sneutrinos $\tilde{\nu}$. Recently, new measurements [12] have failed to reproduce the low-energy $\bar{p}$ flux claimed previously, and have instead established upper limits on the flux which are more than an order of magnitude below the previous claim. We study the question whether these new observations impose significant constraints on relic particle models, and also examine whether upper limits on the fluxes of positrons or gamma rays could constrain such models.

For each relic particle χ that we consider, we fix its total annihilation cross-section $\sigma_{\chi\chi}$ by requiring that its present cosmological density give closure [15]: $\Omega_\chi \equiv \rho_\chi/\rho_c = 1$. These values of $\sigma_{\chi\chi}$ are significantly smaller than some

used in the literature [8]. We calculate the differential $\bar{p}$, e^+ and γ fluxes using a Monte Carlo programme with parameters adjusted to fit e^+e^- annihilation data [16]. We find $\bar{p}$ spectra that are smaller than those used previously, especially in the case of the $\bar{b}b$ final states that are important in $\tilde{h}\tilde{h}$ (and to a lesser extent $\tilde{\gamma}\tilde{\gamma}$) annihilations. Moreover, the spectra have different shapes and do not scale as functions of $E_{\bar{p}}/m_\chi$. We combine these particle physics calculations with the observational upper bounds [12] on the $\bar{p}$ flux to give upper limits on the combination $\rho_\chi^h\sqrt{\tau_{\bar{p}}}$ of astrophysical quantities - ρ_χ^h being the local halo dark matter density and $\tau_{\bar{p}}$ the time of $\bar{p}$ confinement in the galactic magnetic field. For all values of the relic $\tilde{\gamma}$ or $\tilde{h}$ masses, we find upper limits on $\rho_\chi^h\sqrt{\tau_{\bar{p}}}$ which are much larger than the values expected from astrophysics [17]. Thus no range of relic $\tilde{\gamma}$ or $\tilde{h}$ masses is excluded by present $\bar{p}$ data, and the same conclusion holds for present e^+ data [18]. We also discuss the prospects for relic detection by possible future $\bar{p}$ experiments, and possible future constraints on sparticles from cosmic γ rays, presenting both the expected shapes of γ ray spectra and best guesses for their normalizations.

The central formula for the flux observable at the Earth of $\bar{p}$'s produced by relic $\chi\chi$ annihilation in the halo is [7,8]

$$\phi_{\bar{p}}(E_{\bar{p}}) = \frac{1}{4\pi}\langle\sigma_{\chi\chi}v_\chi\rangle_A N_{\bar{p}} f_{\bar{p}}(E_{\bar{p}})\left(\frac{\rho_\chi}{m_\chi}\right)^2 \tau_{\bar{p}} \qquad (1)$$

where $\langle\sigma_{\chi\chi}v_\chi\rangle_A$ is the velocity-averaged $\chi\chi$ annihilation cross-section, $v_{\bar{p}}$ is the interstellar $\bar{p}$ velocity, $f_{\bar{p}}(E_{\bar{p}})$ is the differential cross-section for inclusive $\bar{p}$ production

$$f_{\bar{p}}(E_{\bar{p}}) = \frac{dN}{dE_{\bar{p}}} \equiv \frac{1}{\sigma_{\chi\chi}}\frac{d\sigma(\chi\chi\to\bar{p}+X)}{dE_{\bar{p}}} \qquad (2)$$

suitably modulated by the solar wind, and $\tau_{\bar{p}}$ is the $\bar{p}$ confinement time. We will now discuss each of these factors in turn, and then the analogous formulae for the e^+ and γ fluxes.

The annihilation cross-section for χ's in the halo is controlled by model parameters: mostly by sparticle masses if $\chi = \tilde{\gamma}$, and by the ratio v_1/v_2 of Higgs v.e.v.'s giving masses to the up- and down-type quarks if $\chi = \tilde{h}$. The values of these parameters often used in the literature [8] give large annihilation cross-sections and thus relatively large $\bar{p}$ fluxes $\phi_{\bar{p}}$. However, these same model parameters also control the annihilation rate of χ's in the early Universe, and hence the cosmological relic density ρ_χ of χ's, which we express in units $\Omega_\chi \equiv \rho_\chi/\rho_c$ of the critical density ρ_c. The annihilation cross-section in the early Universe,

averaged at a temperature $T \ll m_\chi$, is given by [3]

$$\langle \sigma_{\chi\chi} v_\chi \rangle_A^T = a + b\left(\frac{T}{m_\chi}\right) + \mathcal{O}\left(\frac{T}{m_\chi}\right)^2 \tag{3a}$$

where a and b are determined by the model parameters, whereas the halo annihilation cross-section

$$\langle \sigma_{\chi\chi} v_\chi \rangle_A = a\left(1 + \mathcal{O}(v_\chi^2)\right) \tag{3b}$$

where the relevant velocities $v_\chi \sim 10^{-3}c$ are very small. For 5 GeV $\lesssim m_\chi \lesssim$ 30 GeV, the cosmological relic χ density is related to the annihilation cross-sections (3) by [3]

$$\Omega_\chi h^2 \simeq \frac{10^{-26}\,\mathrm{cm}^3\,\mathrm{s}^{-1}}{20 x_f (a + \frac{1}{2} b x_f)} \simeq \left(\frac{10^{-26}\,\mathrm{cm}^3\,\mathrm{s}^{-1}}{\langle \sigma_{\chi\chi} v_\chi \rangle_A}\right)\left[20 x_f \left(1 + \frac{1}{2}\frac{b}{a} x_f\right)\right]^{-1} \tag{4}$$

where h is the present-day Hubble constant in units of 50 $\mathrm{kms}^{-1}\mathrm{Mpc}^{-1}$, and x_f is the ratio of the freeze-out temperature T_f in the early Universe to m_χ. Equation (4) gives a close connection between Ω_χ and $\langle \sigma_{\chi\chi} v_\chi \rangle_A$, because $x_f \sim 1/20$ and b/a are fairly model-independent. For example, if $\tilde{\gamma} = \chi$ we find

$$\frac{1}{2}\frac{b}{a} x_f = \left(\sim \frac{1}{40}\right)\left(\frac{m_{\tilde{\gamma}}}{\mathrm{GeV}}\right)^2 \tag{5}$$

We shall assume that the relic χ's are the dominant form of dark matter in the Universe, and shall fix the numerical values of the model parameters by requiring $\Omega_\chi = 1$, as suggested by naturalness and by inflation [15]. We note that model parameters used in the past [8] give relatively low values of the cosmological relic density, $\Omega_\chi \sim 0.2$ to 0.05, so Eq. (4) tells us that our $\langle \sigma_{\chi\chi} v_\chi \rangle_A$ and hence our fluxes will be reduced by a factor ~5 to 20.

The $\bar{p}$'s, e^+'s and γ's are produced indirectly via the annihilation reactions $\chi\chi \to \bar{f}f$: f = τ,c or b for the χ candidates we consider. When f = τ, e^+'s and γ's may be produced either directly or indirectly in the τ decay chain, but no $\bar{p}$'s are produced. When f = c or b, $\bar{p}$'s may be produced either directly in the fragmentation process, or indirectly in the decay chains of heavier particles, just as e^+'s and γ's are produced in the decays of fragmentation particles. It is therefore impossible to calculate these spectra analytically. Since the $\chi\chi \to \bar{f}f$ reaction is similar to $e^+e^- \to \bar{q}q$, a natural possibility is to use e^+e^- data [8] to determine the spectrum $f_{\bar{p}}(E_{\bar{p}})$ of Eq. (1) [and analogously $f_{e^+,\gamma}(E_{e^+,\gamma})$]. However, the e^+e^-

data require three important corrections to meet our purpose.

1) The $\chi\chi \to \bar{f}f$ annihilation fractions are in general quite different from the mix of $\bar{q}q$ final states in e^+e^- annihilation. This can be an important effect, because the $c \to D$ and $b \to B$ meson fragmentation functions are known to be substantially harder than those of the lighter quarks, leaving on the average less energy available for the production of other fragmentation particles in $\bar{c}c$ and $\bar{b}b$ final states. Therefore, one would expect, for example, the $\bar{p}$ spectra from the $\chi\chi$ annihilations considered here to be somewhat softer, and the overall yield of $\bar{p}$'s to be less, than the e^+e^- data.

2) The second difference from e^+e^- annihilation is that particles which are usually considered to be stable in an accelerator experiment (e.g., $\pi^\pm$, $K^\pm$, $\mu^\pm$, neutrons and antineutrons) have time to decay in flight, making additional contributions to the inclusive spectra (dN/dx): $x \equiv E_i/m_\chi$.

We obtain the $(dN/dx)_i$ using the Lund Monte Carlo programme [16], which reproduces the available e^+e^- data fairly accurately, making the modifications needed to include the decays of all unstable particles. We have used the Peterson et al. [19] form of fragmentation function of the c and b quarks, with ε_c and ε_b adjusted to give $\langle z_c \rangle = 0.65$ and $\langle z_b \rangle = 0.81$ as inferred from e^+e^- data. The inclusive distributions $(dN/dx)_i$ are determined for the τ, c and b final states separately, and fit to the functional form

$$\left(\frac{dN}{dx}\right)_i = \beta_i C_i \sum_{j=1}^{2 \text{ or } 3} A_i^j e^{-B_i^j x} \qquad (6)$$

The values of the fit parameters A_i^j, B_i^j and C_i are given in the Table. The shapes of the $(dN/dx)_i$ distributions are relatively insensitive to the centre-of-mass energy. For the γ's and e^+s, there is some increase at low x ($x \lesssim 0.05$) with increasing centre-of-mass energy. However, we will show that the most favourable signal-to-noise region for the e^+'s and γ's is most likely to be in the range $x \gtrsim 0.1$ where this effect is considerably smaller. By choosing a 20 GeV centre-of-mass energy (corresponding to the central m_χ value of 10 GeV) to fit the parameters in the Table, we limit the errors in the spectrum due to these scaling violation to less than ~30% over the interesting range of m_χ. In light of the other uncertainties, a more exact treatment of the spectra is hardly justified. For the $\bar{p}$'s the shapes of the $(dN/dx)_i$ distributions are well described by Eq. (6) for the energy ranges considered here, but the overall normalization, C_i, have a significant dependence on the centre-of-mass energy. This is taken into account by an energy-dependent pre-factor which scales the C by the appropriate amount relative to the $m_\chi = 10$ GeV fits.

Figure 1 shows a Monte Carlo histogram of the $(dN/dx)_i$ weighted by their fractions in $\tilde{\gamma}\tilde{\gamma}$ annihilation for $m_{\tilde{\gamma}} = 10$ GeV, superimposed by a similarly weighted combination of the fits (6) to the $(dN/dx)_i$. Also shown is a function used in previous estimates [8] of the $\bar{p}$ flux. We note that it has a slower fall-off with x than our fit*), and a larger overall normalization. Indeed it gives 1.14 $p,\bar{p}$ per e^+e^- annihilation event at $E_{cm} = 34$ GeV, whereas TASSO [20] observes 0.76±0.06 p, $\bar{p}$ and our Monte Carlo gives 0.72 $p,\bar{p}$ per e^+e^- annihilation event. Also shown in Fig. 1 is dN/dx for $\tilde{h}\tilde{h}$ annihilation for $m_{\tilde{h}} = 10$ GeV.

3) The produced particle spectra must be corrected for propagation through the interstellar medium, and for modulation by the solar wind. The former are expected to be small for $\bar{p}$'s in the energy range of interest here, but the raw spectra of Fig. 1 and the Table must be corrected for modulation by the solar wind. We make this correction using the simplified approach of Perko [21], which has been shown to give an accurate form for the cosmic ray proton spectrum. This approach approximates the diffusion coefficient by $A\beta p$ for $p > p_c$, and by $A\beta p_c$ for $p < p_c$, where the transition momentum $p_c = 1.015$ GeV. The $\bar{p}$ production energy $E_{\bar{p}}$ is then related to the observed energy E by

$$E_{\bar{p}} = E + \Delta E \quad : \text{ for } p > p_c \tag{7a}$$

$$E_{\bar{p}} = p_c \ln\frac{p+E}{p_c+E_c} + E_c + \Delta E \quad : \text{ for } p < p_c \tag{7b}$$

where ΔE is an energy shift that depends on the phase in the solar cycle, and $E = m_{\bar{p}} + T = (m_{\bar{p}}^2+p^2)^{\frac{1}{2}}$. We follow Ref. [12] by choosing $\Delta E = 495$ MeV to correspond to the phase at which their data were taken.

In order to compare these data with the predictions of different models, the latter would have to be normalized by choosing values for the astrophysical quantities ρ_χ^h and $\tau_{\bar{p}}$ in Eq. (1). The local density of halo dark matter is constrained by a variety of astronomical observations. If galaxies form within pre-existing haloes of dark matter, as is widely believed, then dynamical estimates imply [17]

$$0.2\ \text{GeV cm}^{-3} \lesssim \rho_\chi^h \lesssim 0.43\ \text{GeV cm}^{-3} \tag{8}$$

if the fraction F of dissipational matter lies in the range $0.05 \lesssim F \lesssim 0.2$ implied by observations. The range (8) includes most mass-model estimates of ρ_χ^h. For the

---

*) For this reason, there is no sharp cut-off in the $\bar{p}/p$ ratio at $E_{\bar{p}} = m_\chi$ as previously suggested [8], and higher energy $\bar{p}$ data give less stringent limits on sparticles.

best-guess value $F \simeq 0.1$, the local halo density $\rho_\chi^h \simeq 0.3$ GeV cm^{-3} [17]. It has been noted that ρ_χ^h would be significantly higher if the dark matter had the same velocity dispersion as extreme population II stars [22]. However, this does not seem likely if galaxies were formed by dissipational contraction within dark matter haloes. Our best-guess value $\rho_\chi^h \simeq 0.3$ GeV cm^{-3} for the local halo density is considerably smaller than values (0.75 to 1 GeV cm^{-3}) used previously [8] in this context. Thus our fluxes will be reduced by factors ~6 to 10. Strictly speaking, the value of ρ_χ that appears in Eq. (1) is the mean value of ρ_χ within the dark halo weighted by the relative probabilities that $\bar{p}$'s produced at different locations in the halo will diffuse through the galactic magnetic field to reach the Earth. We shall take $\rho_\chi = \rho_\chi^h$ in Eq. (1), and put the effects of the inhomogeneity of ρ_χ into $\tau_{\bar{p}}$, thereby following previous work [7,8].

The propagation of charged particles in the galaxy is not well understood [23], and their confinement time is uncertain and may well be energy-dependent [24]. We will discuss two essentially different models for confinement: disk and halo confinement. For disk confinement, $\tau^d \simeq 10^7$yr, as suggested by the abundances of both stables [24] and unstable (e.g., ^{10}Be) isotopes [25].

We contemplate two types of halo confinement. For type I halo confinement, the local density of cosmic rays is dominated by an old halo population, in which case the age of ^{10}Be is given by the geometric mean of the ^{10}Be half-life and the halo confinement time, τ^h [26]. This suggests $\tau^h \simeq 5\times10^7$yr and a halo thickness ~ 1-2kpc, roughly five times the disk scale height. For type II halo confinement, the local density of cosmic rays is dominated by a young disk population, as in a disk model. However, a longer τ^h is not ruled out so long as the older population does not contaminate the isotope abundances successfully given by the disk model. We approximate the average residence time for an old cosmic ray in the disk b the probability of finding it there, $\tau^{res} = \tau^h V^d/V^h$. Requiring $\tau^{res} < 10^7$yr to avoid contamination, we conclude $\tau^h < 3\times10^8$yr, where we estimate $V^d/V^h \sim 1/30$ as the ratio of the disk scale height to the core size of the dark matter distribution.

Another model is motivated by evidence [14,27] that a substantial fraction (10 to 50%) of the cosmic rays must have passed through much higher grammage (~100gcm^{-2}), if the observations [28] of $\bar{p}$'s at several GeV*) are interpreted as due to secondary production by nuclear interactions of cosmic ray primaries with interstellar gas. This enhancement in path length may be ascribed to halo confinement in a closed box model for the galactic cosmic rays that leak out of the spiral arms where they are produced and spend ~10^7y. The resulting old component has a

---

*) It is desirable to repeat these observations with better particle identification.

lifetime $\sim 7\times10^9 (0.01\text{cm}^{-3}/n_H)$ y, where n_H is the neutral Hydrogen density in atoms cm^{-3}, which is close to the maximum confinement time $\sim 1.5\times10^{10}$y given by the age of the galaxy*).

We shall not restrict our attention to a particular confinement model, but instead consider a range for τ that embraces the three models considered above. These vary through $0.02 \lesssim \hat{\tau}_{p}^{-} \lesssim 200$ for $\hat{\tau}_{p}^{-} \equiv \tau_{p}^{-}/2\times10^{15}$s. Probably $0.15 \lesssim \hat{\tau}_{p}^{-} \lesssim 5$, but the confinement time τ_{p}^{-} remains as the most uncertain of the ingredients in Eq. (1).

We present in Fig. 2 numerical estimates of the $\bar{p}/p$ ratio derived**) from the $\bar{p}$ flux in a sampling of supersymmetric models, based on the default options $\rho_\chi^h = 0.3$ GeVcm^{-3} and $\tau_{p}^{-} = 2\times10^{15}$s. We see that because of the large reduction factors mentioned earlier, due mainly to the assumed values of $\langle\sigma_{\chi\chi} v_\chi\rangle_A$ and ρ_χ^h, the improved upper limit

$$\frac{\int_{205\,\text{MeV}}^{640\,\text{MeV}} dE_{\bar{p}}\, \phi_{\bar{p}}(E_{\bar{p}})}{\int_{205\,\text{MeV}}^{640\,\text{MeV}} dE_{p}\, \phi_{p}(E_{p})} < 4.6\times10^{-5}\ (85\%\ \text{C.L.})$$

recently reported [12] does not impose any significant constraint on supersymmetric particle models. Indeed, they might even give fluxes considerably below the curves in Fig. 2, since some of the halo dark matter could be baryonic, and τ_{p}^{-} could be shorter than 2×10^{15}s, as discussed above. For this reason, we prefer to use the data of Ref. [12] to quote upper limits on the quantity $\hat{\rho}_\chi^h \sqrt{\hat{\tau}_{p}^{-}}$, where $\hat{\rho}_\chi^h \equiv \rho_\chi^h/0.3$ GeVcm^{-3}. Figure 3 shows upper limits on $\hat{\rho}_\chi^h \sqrt{\hat{\tau}_{p}^{-}}$ for $\chi = \tilde{\gamma}$ and $\tilde{h}$, as functions of m_χ. These results were derived assuming an energy-independent mean free path-length which is likely to be the case for $E_{p}^{-} \lesssim 5$ GeV [23]. Although these limits are not as stringent as the upper limits on ρ_χ^h from the non-observation of high-energy solar neutrinos [27], they are much stronger than the available upper limits on the local halo density of axions [28].

---

*) A possible test of this model could be the observation of a halo component in the γ data, with an energy spectrum consistent with that for the decay of π^0's from nuclear interactions.

**) We use the p flux from Ref. [21] with $\Delta E = 495$ MeV [12].

It should be noted that even a positive signal for low-energy $\bar{p}$'s would not provide a "smoking gun" for relic annihilations. This is because of a possible background from supernovae buried deep in dense interstellar clouds [29]. They could generate high-energy primary cosmic rays which produce $\bar{p}$'s that are initially above the kinematic threshold of several GeV but subsequently decelerated adiabatically. One could produce in this manner a low-energy $\bar{p}$ flux close to the new upper limit even if only (3 or 4%) of cosmic ray nucleons were produced in this manner. This translates into requiring ~10% of all supernova explosions to occur in such dense clouds, which is well within the experimental uncertainties [30].

Also shown in Fig. 3 are upper limits on $\hat{\rho}_\chi^h \sqrt{\tau_{e^+}}$ from a comparison of the observed flux of high-energy cosmic ray e^+'s with the flux expected from $\chi\chi$ annihilation. The analysis*) of the e^+ spectrum is similar to that of the $\bar{p}$'s discussed above, but the following two points merit comment. a) There is a significant contribution to the e^+ spectrum from particles (e.g., $\pi^+, \mu^+, \bar{n}$) which appear stable in e^+e^- experiments, but must be allowed to decay in our case**). b) Energy loss during propagation through the interstellar medium is significant for e^+'s, unlike the $\bar{p}$ case. The loss rate can be written as [32]

$$\frac{dE}{dt} = -\left(2.7\, n_H + 7.3\, n_H E + (U_{rad} + U_{mag}) E^2\right) \cdot 10^{-16}\ \mathrm{GeV\,s^{-1}} \qquad (9)$$

where U_{rad} is the ambient photon energy density in $\mathrm{eVcm^{-3}}$, and E is the e^+ energy in GeV. The four terms in (9) represent the energy losses due to ionization, bremsstrahlung, inverse Compton scattering and synchrotron radiation respectively. None of the terms is negligible for e^+'s of energy $E \sim 1$ GeV in the galactic disc ($n_H \sim 0.3$ atoms $\mathrm{cm^{-3}}$, $U_{rad} \sim 2$ $\mathrm{eVcm^{-3}}$, $U_{mag} \sim 0.5$ $\mathrm{eVcm^{-3}}$). However, the e^+'s spend most of their time, and lose most of their energy, in the halo outside the disc, where $n_H \sim 0.01$ atoms $\mathrm{cm^{-3}}$, $U_{rad} \sim 0.25$ $\mathrm{eVcm^{-3}}$ and $U_{mag} \sim 0.05$ $\mathrm{eVcm^{-3}}$, so that inverse Compton scattering is dominant for $E \gtrsim 1$ GeV. The e^+ spectra produced in $\chi\chi$ annihilation have been corrected for these energy losses assuming halo

---

*) Similar Monte Carlo calculations of the e^+ spectra have been made by Tylka and Eichler [31], so our discussion here will be brief.

**) For ease of computation, we have neglected polarization effects on these decay spectra, which could change them by a factor $\lesssim 2$.

confinement*), and for the modulation by the solar wind [21], and then compared with observation [18] to produce the e^+ constraints on $\hat{\rho}^h_\chi \sqrt{\tau_{e^+}}$ shown in Fig. 3. We only use the data for $E_{e^+} \gtrsim 2$ GeV, since the model curves at lower energies rise much more slowly than the observed e^+ flux, so that the lower energy data would give a less stringent bound on $\hat{\rho}^h_\chi \sqrt{\tau_{e^+}}$ **). Our "bounds" were obtained by demanding that the models give a smaller flux than a simple power-law fit to the data above 2 GeV. We see that they are somewhat less stringent than the $\bar{p}$ limits. Moreover, for the reasons discussed above, more care should be exercised in interpreting the e^+ limits. For one thing, as mentioned above the diffusion of relativistic cosmic ray nucleons may be energy-dependent [24], suggesting that relativistic electrons could have an energy-dependent path length $\propto E^{-0.5\pm0.1}$. Another point is that there must be a secondary e^+ yield from the nuclear interactions of primary matter cosmic rays [33]. Therefore an anomalous $e^+/(e^-+e^+)$ ratio also could not be interpreted as a "smoking gun" for relic annihilations.

Finally, we discuss the γ spectra from $\chi\chi$ annihilation. As in the cases of the $\bar{p}$'s and e^+'s, we include in our γ spectra $f(E_\gamma)$ the decays of all unstable particles. Clearly there are no energy losses on the way to the Earth. The confinement time τ in Eq. (1) is replaced by an integral over the line-of-sight which depends on the galactic latitude b and longitude ℓ [34]. The γ-ray flux may be approximated by

$$\Phi_\gamma(E) = \frac{1}{4\pi}\langle\sigma_{\chi\chi} v_\chi\rangle f_\gamma(E_\gamma)\left(\frac{\rho_\chi}{m_\chi}\right)^2 a\, I(b,\ell)$$

$$= \frac{1.6\times10^{-6}}{cm^2\,s\,sr\,GeV}\left(\frac{\rho^h_\chi}{0.3\,GeV\,cm^{-3}}\right)^2\left(\frac{\langle\sigma_{\chi\chi} v_\chi\rangle_A}{10^{-26}\,cm^3\,s^{-1}}\right)\left(\frac{m_\chi}{GeV}\right)^{-2}\left(\frac{a}{7\,kpc}\right)\left(\frac{f(E_\gamma)}{GeV^{-1}}\right) I(b,\ell) \qquad (10)$$

where we assume a halo density of the form

$$\rho_\chi = \rho^h_\chi\left(\frac{a^2 + r_0^2}{a^2 + r^2}\right) \qquad (11)$$

so that

---

*) The effect of neglecting energy losses in the disk is to overestimate somewhat the positron flux.

**) This would not be the case for smaller values of m_χ, but closure cannot be reached for $m_{\tilde{n}} \lesssim 5$ GeV, and values of the slepton and squark masses which conflict with experimental limits would be required to obtain closure for $m_{\tilde{\gamma}} \lesssim 3$ GeV [15].

$$I(b,\ell) = \frac{\beta}{2}\left[\frac{1+\alpha^2}{\beta^2}\right]^2\left\{\frac{\pi}{2} + \frac{\alpha\beta}{1+\alpha^2}\cos b\cos\ell + \tan^{-1}\left[\frac{\alpha}{\beta}\cos b\cos\ell\right]\right\} \quad (12)$$

where $\alpha \equiv r_0/a$ and $\beta^2 = 1+\alpha^2 - \alpha^2\cos^2 b\cos^2\ell$. The factor $I(b,\ell)$ (12) varies between 1.24 ($b = 90°$: the galactic pole), 9.01 ($b = 0°$, $\ell = 0°$: the galactic centre) and 0.61 ($b = 0°$, $\ell = 180°$: the anticentre). We show in Fig. 4 the γ fluxes for $b = 90°$ and $\chi = \tilde{\gamma}$ and $\tilde{h}$.

These predicted diffuse γ-ray fluxes are to be compared with that observed [35] for $E_\gamma >$ (35 to 200) MeV, which consists of two components: an isotropic component fitted by $\phi_\gamma(E) = 2.8\times10^{-8}E^{-3.4}\,cm^{-2}s^{-1}sr^{-1}GeV^{-1}$, and a disc component fitted by $\phi_\gamma(E) = 2.8\times10^{-6}E^{-1.6}(\sin|b|)^{-1}cm^{-2}s^{-1}sr^{-1}GeV^{-1}$. The galactic disc component dominates the observed background for $E > 80(70)$ MeV at $|b| = 90°(60°)$ and is plotted in Fig. 4 for $|b| = 90°$. Since the slopes of the theoretical spectra become equal to that of the background spectrum at energies $E \gtrsim 0.1$ GeV, we compare theory with experiment in this range of energies. Demanding that the predicted flux spectra be bounded above by this disc component implies $\hat{\rho}^h_\chi\sqrt{a/7\ kpc} \lesssim 5.3(14,60)$ for $m_{\tilde{\gamma}} = 3(6,16)$ GeV, which is less stringent than the corresponding $\bar{p}$ limit for $\hat{\tau}_{\bar{p}} = 1$. This is a conservative limit: e.g., taking account of the angular dependence could improve our constraint on $\hat{\rho}\sqrt{a}$, but this would require knowledge of the halo density close to the core. Future experiments such as the Gamma Ray Observatory (GRO) will enable one to improve further this limit.

In addition to the broad band spectrum, it has been suggested [36] that there might be significant DM annihilation into a vector meson V and a single photon, thus producing a narrow-band photon spectrum that might be observable. The branching ratio for this process has been estimated [37] to be $\Gamma_{V\gamma}/\Gamma_{q\bar{q}} \sim 2\times10^{-4}$ $(3\ GeV/m_\chi)^2$ for $V = J/\psi$, and $\sim1.5\times10^{-5}$ $(10\ GeV/m_\chi)^2$ for $V = \Upsilon$, where $\Gamma_{q\bar{q}}$ is the total branching ratio for χ annihilation into the corresponding $q\bar{q}$ pair. Unfortunately, we estimate that the signal/background for this process, relative to that for the broad band, π^0-produced γ's, is $(S/B)_V/(S/B)_{\pi^0} \sim 36(GeV/m_\chi)^2$, thus only for relatively light χ does the narrow-band signal look at all promising.

The new low-energy cosmic ray $\bar{p}$ limit [12] does not set, by itself, any significant constraint on relic halo particles. Current models could give a $\bar{p}$ signal just below the new limit, but astrophysical uncertainties, especially in containment time, render our predictions uncertain by some four orders of magnitude. Storage times in the halo could even be as long as $\sim10^{10}$ y, in which case relic signatures should be present, though buried in the various backgrounds we have discussed. We do not believe it will ever be possible to derive significant limits on supersymmetric relic particles from cosmic ray $\bar{p}$ data alone. A possible

strategy for future experiments is to combine $\bar{p}$ searches with those for e^+'s and γ's. By ensuring that comparable sensitivities to a given relic candidate could be attained for both $\bar{p}$ and e^+, one might circumvent some of the background problems. The merit of the γ search is to remove much of the uncertainty in containment time, but disentangling a signal will require persistence.

REFERENCES

[1] For a recent review, see e.g.:
V. Trimble, Ann. Rev. Astron. Astrophys. 25 (1987) 425.

[2] See, e.g.:
D. Hegyi and K. Olive, Ap.J. 303 (1986) 56.

[3] H. Goldberg, Phys. Rev. Lett. 50 (1983) 1419;
J. Ellis, J.S. Hagelin, D.V. Nanopoulos, K. Olive and M. Srednicki, Nucl. Phys. B238 (1984) 493.

[4] L. Ibañez, Phys. Lett. 137B (1984) 160;
J.S. Hagelin, G.L. Kane and S. Raby, Nucl. Phys. B241 (1984) 638.

[5] M. Goodman and E.Witten, Phys. Rev. D31 (1985) 3059.

[6] J. Silk and M. Srednicki, Phys. Rev. Lett. 55 (1985) 257;
M. Srednicki, K. Olive and J. Silk, Nucl. Phys. B279 (1987) 804.

[7] J. Silk and M. Srednicki, Phys. Rev. Lett. 53 (1984) 624.

[8] F.W. Stecker, S. Rudaz and T. Walsh, Phys. Rev. Lett. 55 (1985) 2622;
S. Rudaz and F.W. Stecker, Ap. J. 325 (1988) 16.

[9] S.P. Ahlen et al., Phys. Lett. B195 (1987) 603;
D.O. Caldwell et al., Santa Barbara preprint UCSB-HEP-88-6 (1988).

[10] Fréjus Collaboration, B. Kuznik, Orsay preprint LAL 87-21 (1987);
IMB Collaboration, J.M. Losecco et al., Phys. Lett. B188 (1987) 388.

[11] J.S. Hagelin, K.-W. Ng and K. Olive, Phys. Lett. 180B (1987) 375;
K.-W. Ng, K. Olive and M. Srednicki, Phys. Lett. 188B (1987) 138.

[12] S.P. Ahlen et al., Phys. Rev. Lett. 61 (1988) 145;
see also T. Bowen et al., Univ. of Arizona preprint (1988).

[13] A. Buffington, S.M. Schindler and C.R. Pennypacker, Ap. J. 248 (1981) 1179.

[14] R.J. Protheroe, Ap. J. 251 (1981) 387.

[15] R. Brandenberger, Rev. Mod. Phys. 57 (1985) 1.

[16] T. Sjöstrand, University of Lund preprint LUTP 85-10 (1985);
For an up-to-date review and comparison with experimental data, see:
T. Sjöstrand, Int. J. Mod. Phys. A3 (1988) 751 and references therein.

[17] R. Flores, CERN preprint TH.4736/87 (1987).

[18] A. Buffington, C.D. Orth and G.F. Smoot, Ap. J. 199 (1975) 669;
R.L. Golden et al., submitted to Astr. Ap. (1986).

[19] C. Peterson, D. Schlatter, I. Schmitt and P.M. Zerwas, Phys. Rev. D27 (1983) 105.

[20] TASSO Collaboration, paper submitted to the 24th International Conference on High Energy Physics, Munich (1988).

[21] J.S. Perko, Astr. Ap. 184 (1987) 119.

[22] J. Binney, A. May and J.P. Ostriker, M.N.R.A.S. 226 (1987) 149.

[23] See, e.g., V.L. Ginzburg and V.S. Ptuskin, Rev. Mod. Phys. 48 (1976) 161;
C.J. Cesarsky, Ann. Rev. Astron. Astrophys. 18 (1980) 289.

[24] J.F. Ormes and R.J. Protheroe, Ap. J. 272 (1983) 756.

[25] M.E. Weidenbeck and D.E. Greiner, Ap.J. 239 (1980) L139.

[26] V.L. Prishchep and V.T. Ptuskin, Astr. Space Sci. 32 (1975) 265.

[27] S.A. Stephens, Nature 289 (1981) 267.

[28] R.L. Golden et al., Phys. Rev. Lett. 43 (1979) 1196.

[29] J. Ellis, R. Flores and S. Ritz, Phys. Lett. B198 (1987) 393.

[30] S. de Panfilis et al., Phys. Rev. Lett. 59 (1987) 839.

[31] V.L. Ginzburg and V.S. Ptuskin, Sov. Ast. Lett. 7 (1981) 325;
L.C. Tan and L.K. Ng, Ap. J. 269 (1983) 751;
S.A. Stephens and B.C. Manger, "High Energy Astrophysics", ed. J. Audouze and J. Tran Thanh Van (Editions Frontières, Gif-sur-Yvette, 1984), p. 217.

[32] J.M. Shull, Ap. J. 237 (1980) 269.

[33] A.J. Tylka and D. Eichler, "Cosmic Ray Positrons from Photino Annihilation in the Galactic Halo", preprint (1988).

[34] M.S. Longair, in "High Energy Astrophysics", (Cambridge Univ. Press, 1981) 278.

[35] R.J. Protheroe, Ap. J. 254 (1982) 391.

[36] J.E. Gunn et al., Ap. J. 223 (1978) 1015;
M.S. Turner, Phys. Rev. D34 (1986) 1921.

[37] C. Fichtel et al., Ap. J. 217 (1977) L9.

[38] M. Srednicki, S. Theisen and J. Silk, Phys. Rev. Lett. 56 (1986) 263.

[39] S. Rudaz, Phys. Rev. Lett. 56 (1986) 2128.

Table

Fit parameters describing the spectra obtained from the Monte Carlo, with m_χ = 10 GeV using the functional form $dN/dx = C\beta\Sigma_j A_j \exp(-B_j x)$.

	C	A_1	B_1	A_2	B_2	A_3	B_3
$\bar{p}$ from b	$[(1-25/m_\chi^2)^{\frac{1}{2}}(10\cdot 2/m_\chi+0.151)]$	181	39.1	11.2	13.2	—	—
e^+ from c	$[9.67/m_\chi+0.033]$	378	42.4	16.1	11.5	—	—
e^+ from b	1.0	678	147	200	51.8	11.6	13.1
e^+ from c	1.0	537	160	187	53.4	23.1	18.1
e^+ from τ	1.0	3.49	5.42	14.8	22.3	—	—
γ from b	1.0	989	63.6	94.3	18.5	—	—
γ from c	1.0	607	51.3	80.9	16.3	—	—
γ from τ	1.0	15.8	7.61	5.45	21.5	—	—

FIGURE CAPTIONS

Fig. 1 : Spectra of $\bar{p}$'s produced in relic $\chi\chi$ annihilations. The histogram is the Monte Carlo [16] output for a $\tilde{\gamma}$ weighing 10 GeV, and the solid curve is the result of the corresponding fit (6) for $m_{\tilde{\gamma}} = 10$ GeV. The dash-dotted curve is the result of the fit (6) for $m_{\tilde{h}} = 10$ GeV. Note that it is softer than the $\tilde{\gamma}$ curve because $\tilde{h}\tilde{h} \to \bar{b}b$ has a larger branching fraction than $\tilde{\gamma}\tilde{\gamma} \to \bar{b}b$. The dotted curve is that of Stecker and Rudaz [8] for $m_{\tilde{\gamma}} = 10$ GeV: their curve for $m_{\tilde{h}} = 10$ GeV would be a factor 1.3 higher.

Fig. 2 : Ratios of $\bar{p}$ and p fluxes from different relic candidates, after modulation by the solar wind. Also shown is the recent upper limit on the $\bar{p}$ flux from Ref. [12]. Previous measurements [26] at higher energies are off-scale beyond the top of the figure. The curves are calculated with the default options $\rho_\chi^h = 0.3$ GeVcm^{-3} [17] and $\tau_{\bar{p}} = 2\times10^{15}$s. The solid/dotted/dashed/dash-dotted curves are for $m_{\tilde{\gamma}} = 3$ GeV/$m_{\tilde{\gamma}} = 6$ GeV/$m_{\tilde{\gamma}} = 10$ GeV/$m_{\tilde{h}} = 15$ GeV.

Fig. 3 : Upper limits on $\hat{\rho}_\chi^h\sqrt{\tau_{\bar{p}}}$ from the upper limit of Ref. [12] on the $\bar{p}$ flux, for $\chi = \tilde{\gamma}$ and $\tilde{h}$ as functions of m_χ. Also shown are "upper limits" on $\hat{\rho}_\chi^h\sqrt{\tau_{e^+}}$ from measurements of the e^+ cosmic ray flux above 2 GeV [18]. Lower-energy e^+ data are not competitive for constraining relics in the mass ranges considered here.

Fig. 4 : Fluxes of γ's produced in relic $\chi\chi$ annihilations calculated with the default option $\rho_\chi^h = 0.3$ GeVcm^{-3} and a = 7 kpc. The solid/dotted/dashed/dashed-dotted curves are for $m_{\tilde{\gamma}} = 3$ GeV/$m_{\tilde{\gamma}} = 6$ GeV/$m_{\tilde{\gamma}} = 16$ GeV/$m_{\tilde{h}} = 15$ GeV. Also shown is the disc component of the cosmic γ-ray background [35].

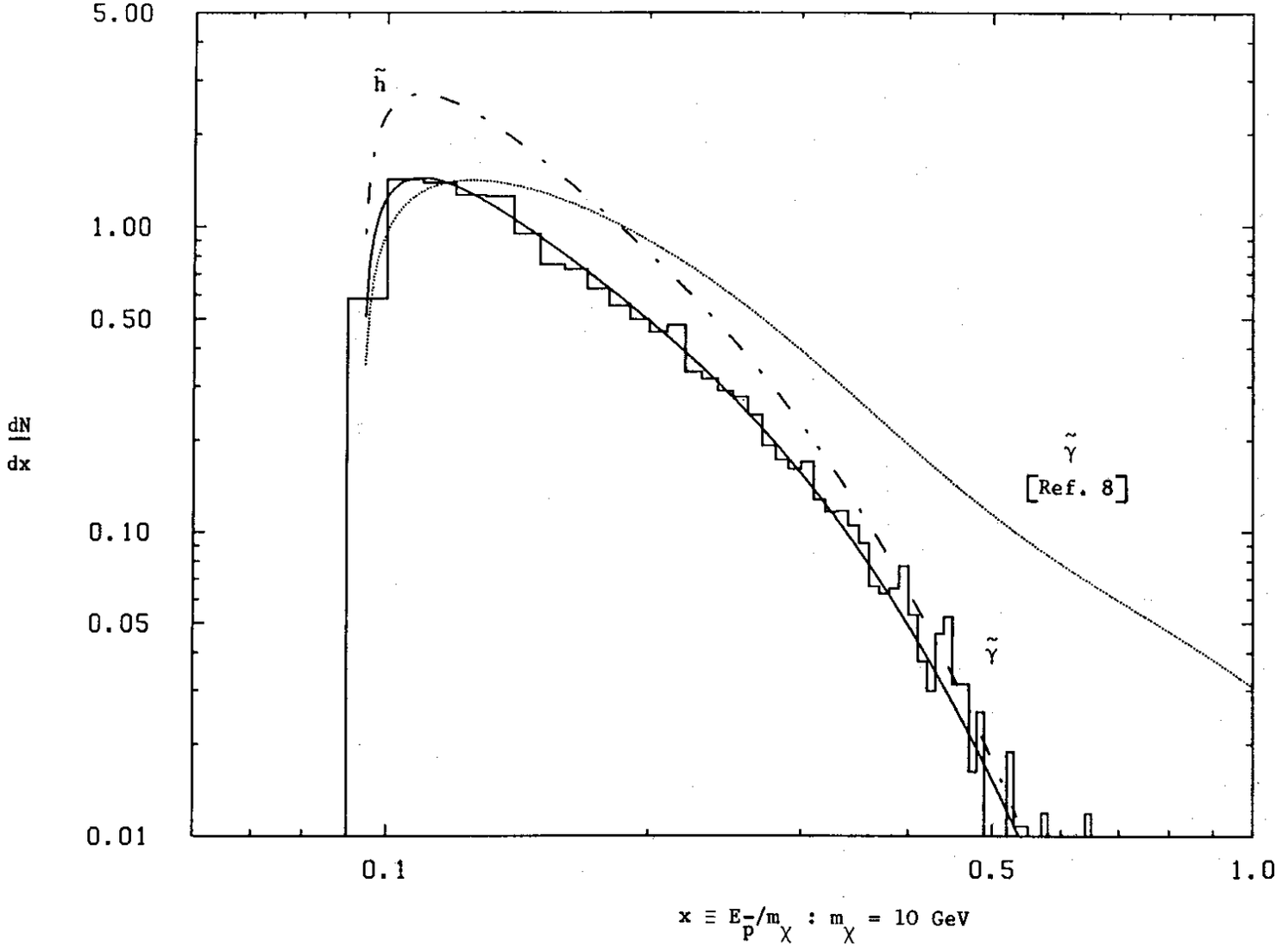

Fig. 1

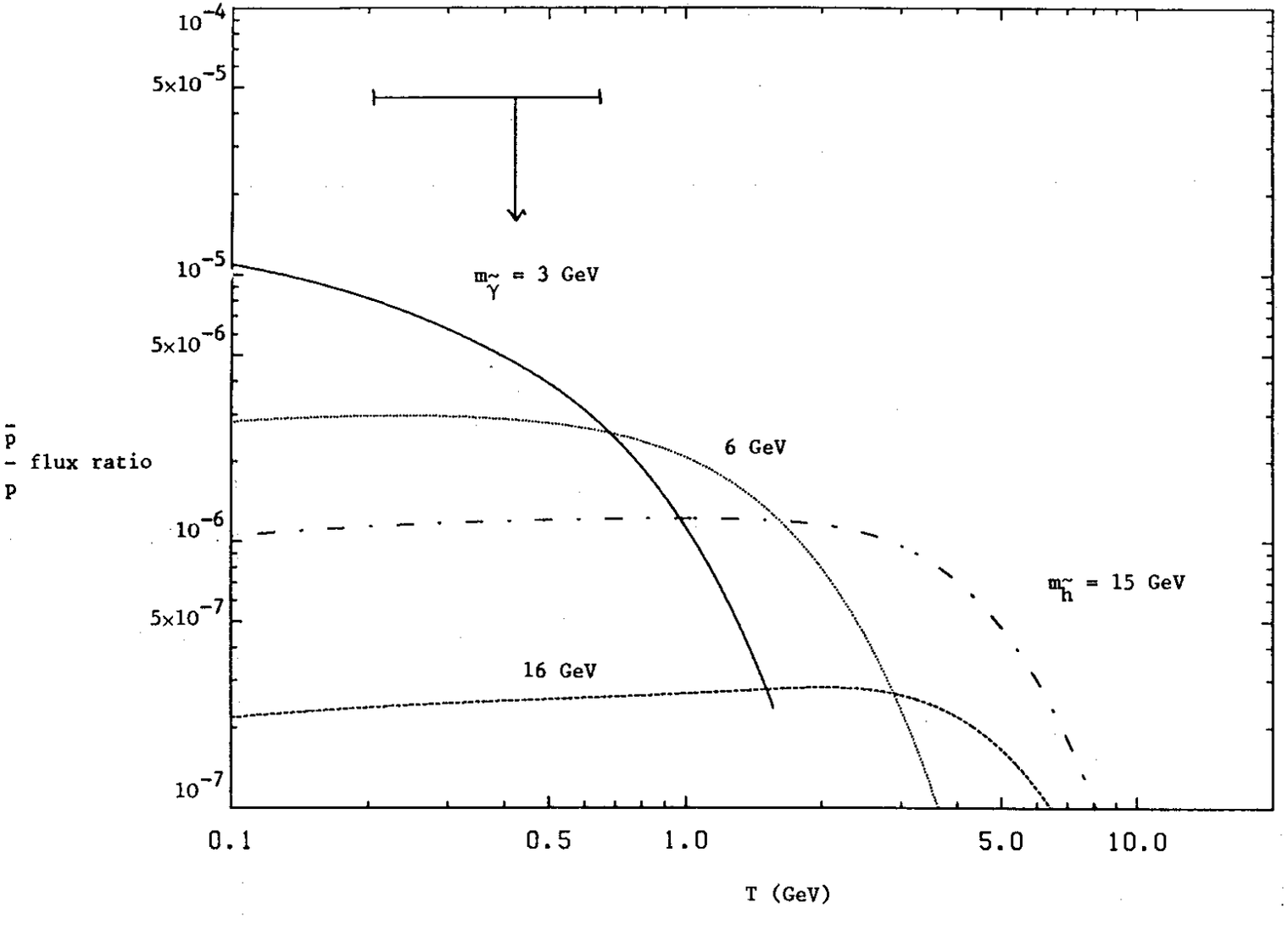
10^{-4}
5×10^{-5}
10^{-5}
5×10^{-6}
10^{-6}
5×10^{-7}
10^{-7}
$\frac{\bar{p}}{p}$ flux ratio
$m_{\tilde{\gamma}}$ = 3 GeV
6 GeV
$m_{\tilde{h}}$ = 15 GeV
16 GeV
0.1
0.5
1.0
5.0
10.0
T (GeV)

Fig. 2

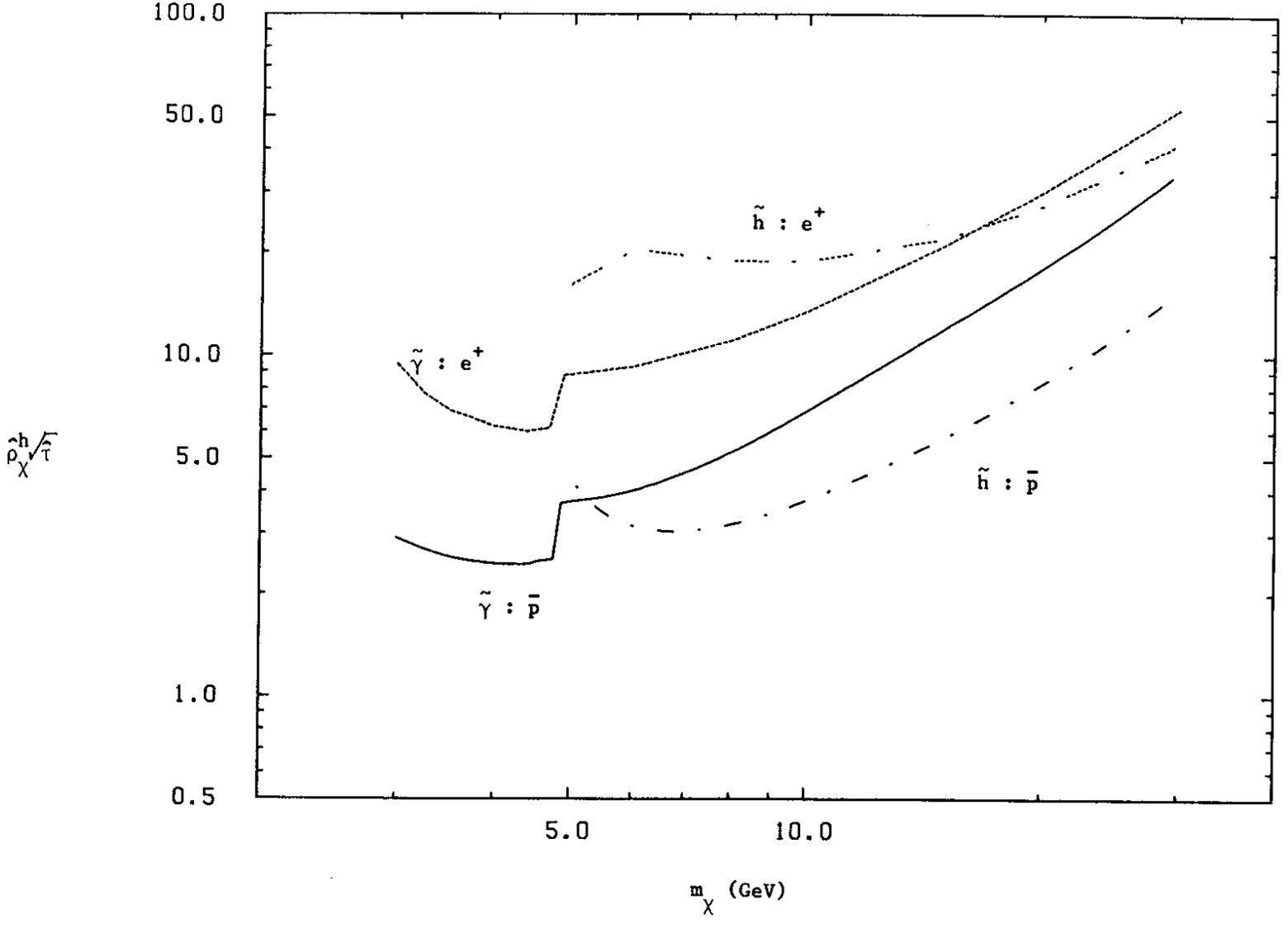
100.0
50.0
10.0
5.0
1.0
0.5
5.0
10.0
$\hat{\rho}^h_\chi \sqrt{\hat{\tau}}$
m_χ (GeV)
$\tilde{h} : e^+$
$\tilde{\gamma} : e^+$
$\tilde{h} : \bar{p}$
$\tilde{\gamma} : \bar{p}$

Fig. 3

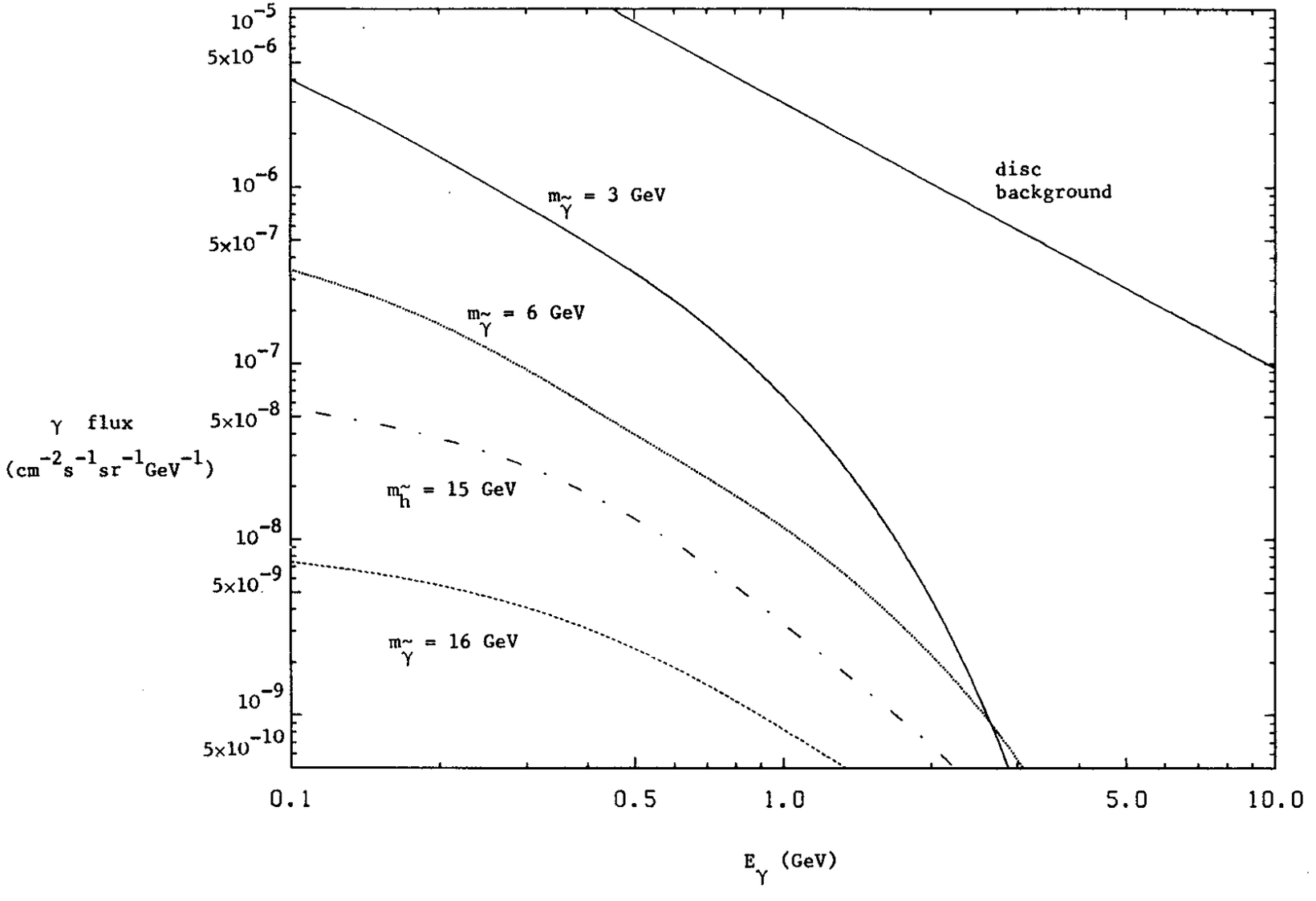
10^{-5}
5×10^{-6}
10^{-6}
5×10^{-7}
10^{-7}
5×10^{-8}
10^{-8}
5×10^{-9}
10^{-9}
5×10^{-10}
γ flux
(cm^{-2}s^{-1}sr^{-1}GeV^{-1})
$m_{\tilde{\gamma}}$ = 3 GeV
disc
background
$m_{\tilde{\gamma}}$ = 6 GeV
$m_{\tilde{h}}$ = 15 GeV
$m_{\tilde{\gamma}}$ = 16 GeV
0.1
0.5
1.0
5.0
10.0
E_γ (GeV)

Fig. 4